Climate Dynamics (2000) 16:917–933

M. Pontaud · J.-P. Céron · M. Kimoto · F. Pluviaud
L. Terray · A. Vintzileos

CoPIVEP: a theory-based analysis of coupled processes and interannual variability in the Equatorial Pacific in four coupled GCMs

Received: 30 July 1999 / Accepted: 25 April 2000

Abstract The interannual variability over the tropical Pacific and a possible link with the mean state or the seasonal cycle is examined in four coupled ocean-atmosphere general circulation models (GCM). Each model is composed of a high-resolution ocean GCM of either the tropical Pacific or near-global oceans coupled to a moderate-resolution atmospheric GCM, without using flux correction. The oceanic subsurface is considered to describe the mean state or the seasonal cycle through the analytical formulations of some potential coupled processes. These coupled processes characterise the zonal gradient of sea surface temperature (hereafter SST), the oceanic vertical gradient of temperature and the equatorial upwelling. The simulated SST patterns of the mean state and the interannual signals are generally too narrow. The grid of the oceanic model could control the structure of the SST interannual signals while the behaviour of the atmospheric model could be important in the link between the oceanic surface and the subsurface. The first SST EOFs are different between the coupled models, however, the second SST EOFs are quite similar and could correspond to the return to the normal state while that of the observations (COADS) could favour the initial anomaly. All the models seem to simulate a similar equatorial wave-like dynamics to return to the normal state. The more the basic state is unstable from the coupled processes point of view, the more the interannual signal are high. It seems that the basic state could control the intensity of the interannual variability. Two models, which have a significant seasonal variation of the interannual variance, also have a significant seasonal variation of the instability with a few months lag. The potential seasonal phase locking of the interannual fluctuations need to be examined in more models to confirm its existence in current tropical GCMs.

M. Pontaud[1] (✉) · J.-P. Céron · F. Pluviaud
Meteo-France, ENM/UFR, 42 av. G. Coriolis,
31057 Toulouse-Cedex, France

M. Kimoto
Center for Climate System Research, University of Tokyo,
4-6-1, Komba, Meguro-ku, Tokyo 153-8904 Japan

L. Terray
CERFACS, 42 av. G. Coriolis, 31057 Toulouse-Cedex, France

A. Vintzileos
Institut Pierre-Simon Laplace, Université Pierre et Marie Curie,
4 place Jussieu, 75252 Paris Cedex 05, France

Present address:
[1] Meteo-France, Direction InterRégionale de la Polynésie Française, BP 6005 Faa'a Aéroport, 98702 TAHITI – Polynésie française
E-mail: marc.pontaud@meteo.fr

1 Introduction

Among the various aspects of ocean-atmosphere coupling, the tropical climate receives much attention. Different coupled ocean-atmosphere models, either global or focusing on this region, are now operating around the world, but the results are not fully satisfactory. Different studies describe tropical air-sea interactions in general circulation models (Neelin et al. 1992; Stockdale et al. 1993; Neelin and Dijkstra 1995; Mechoso et al. 1995, hereafter M95; see also the special issue "Coupled ocean-atmosphere models" in Monthly Weather Review May 1997). In the study M95, 11 coupled ocean-atmosphere models are examined. None of them uses flux correction. The paper focuses on the seasonal cycle over the tropical Pacific. Several biases are shared by some of the participant models: a too strong and too narrow cold tongue; a double ITCZ which does or does not cross the equator; too warm SSTs off the coast of South America; ... Although not devoted to the study of interannual variability M95 mentioned that the "*results of the participant modelers are consistent with the apparent lack of correlation between the success in simulating the seasonal cycle and annual mean and obtaining realistic interannual variability of coupled system*". The con-

Table 1 Model description. Spatial resolution is given as the longitude-latitude grid size or T for triangular spectral resolution. The number of model levels/layers is denoted by L. Key to convection schemes: MF, mass flux; AS, Arakawa-Schubert; DD, downdraughts; SC, shallow-convection; MCC, moisture convergence adjustment; MCA, moist convective adjustment. Key to ocean mixing: Ri, Richardson number dependent; ML, mixed layer; TKE, turbulent kinetic energy closure. Laboratories: MPI, Max-Planck-Institute für Meteorologie; CCSR, Center for Climate System Research; CERFACS, Centre Européen de Recherche et de Formation Avancée en Calcul Scientifique; IPSL, Institut Pierre Simon Laplace

Laboratories	MPI	CCSR	CERFACS	IPSL
Short names	MPI ECHO-2	CCS	CFX	IPS
Atmospheric model	ECHAM-4	CCSR/NIES	ARPEGE	LMD
> Resolution	T42L19	T21L20	T42L30	64 × 50 pts L11
> Convection	MF	AS + DD	MF + SC	MCC + MCA
Oceanic model	HOPE-2	GFDL-MOM	OPA (LODYC)	OPA (LODYC)
> Domain	Global	Global	Pacific	Pacific
> Resolution hor	2.8° × 0.5°–2.8°	2.5° × 0.5°–2.0°	0.75° × 1/3° (eq)	0.75° × 1/3° (eq)
> Resolution ver	L20	L20	L28	L28
> Mixing	Ri + ML	2.5 TKE	1.5 TKE	1.5 TKE
Simulation (years)	20	65	20	29
Reference	Frey et al. (1997)	Kimoto et al. (1997)	Terray (1998)	Vintzileos et al. (1999a, b)
SST	10 m	2 m	Temperature 5 m	Temperature 5 m
T-100 m	100 m	95 m	100 m	100 m
Vertical velocity	87 m	average 0–95 m	average 0–94 m	average 0–94 m

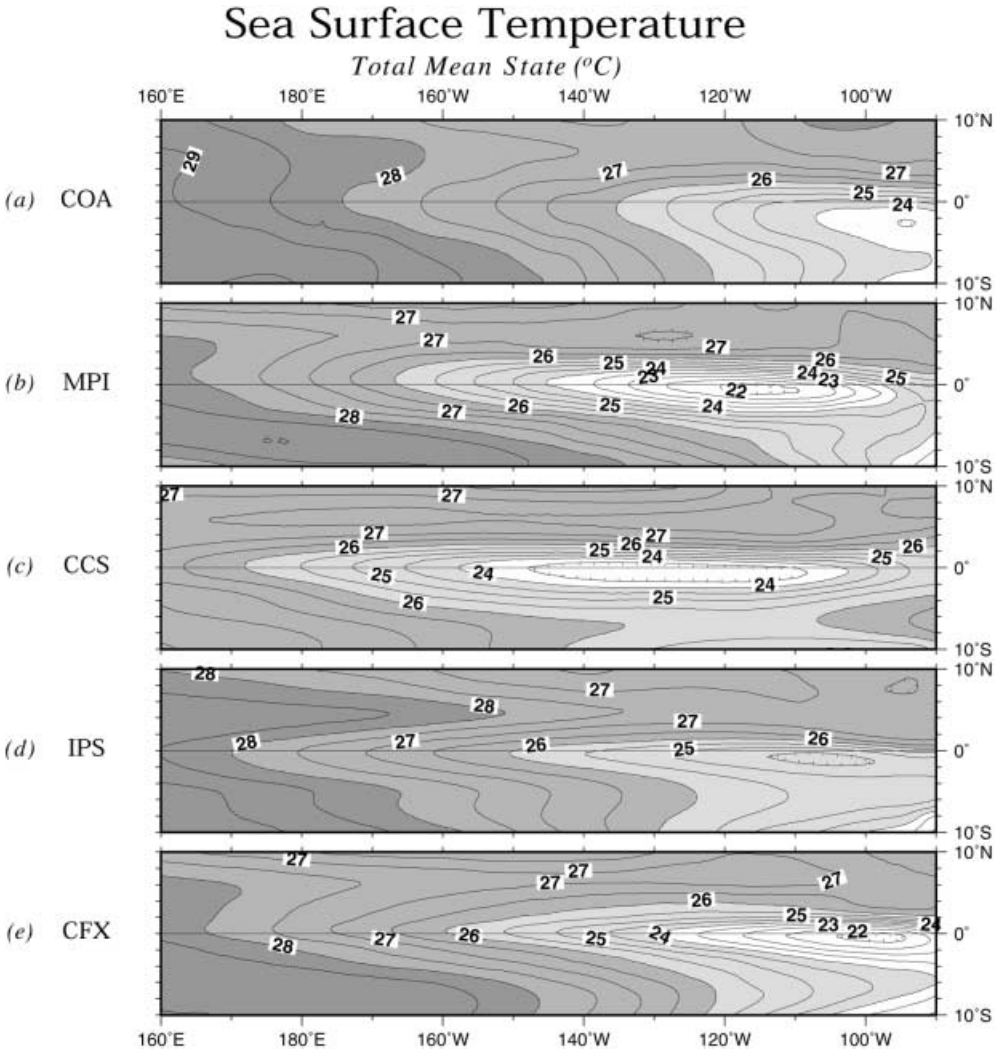

Fig. 1 Sea surface temperature: total mean state (units: °C)

cluding sentence of the paper recommends researchers "*to investigate in detail the relationship between interannual variability and the seasonal cycle in the models*".

Consequently, it was decided (during a workshop of the Coupled GCM Study Group -CGSG- in Paris, 24–28 June 1996) to realise the informal intercomparison

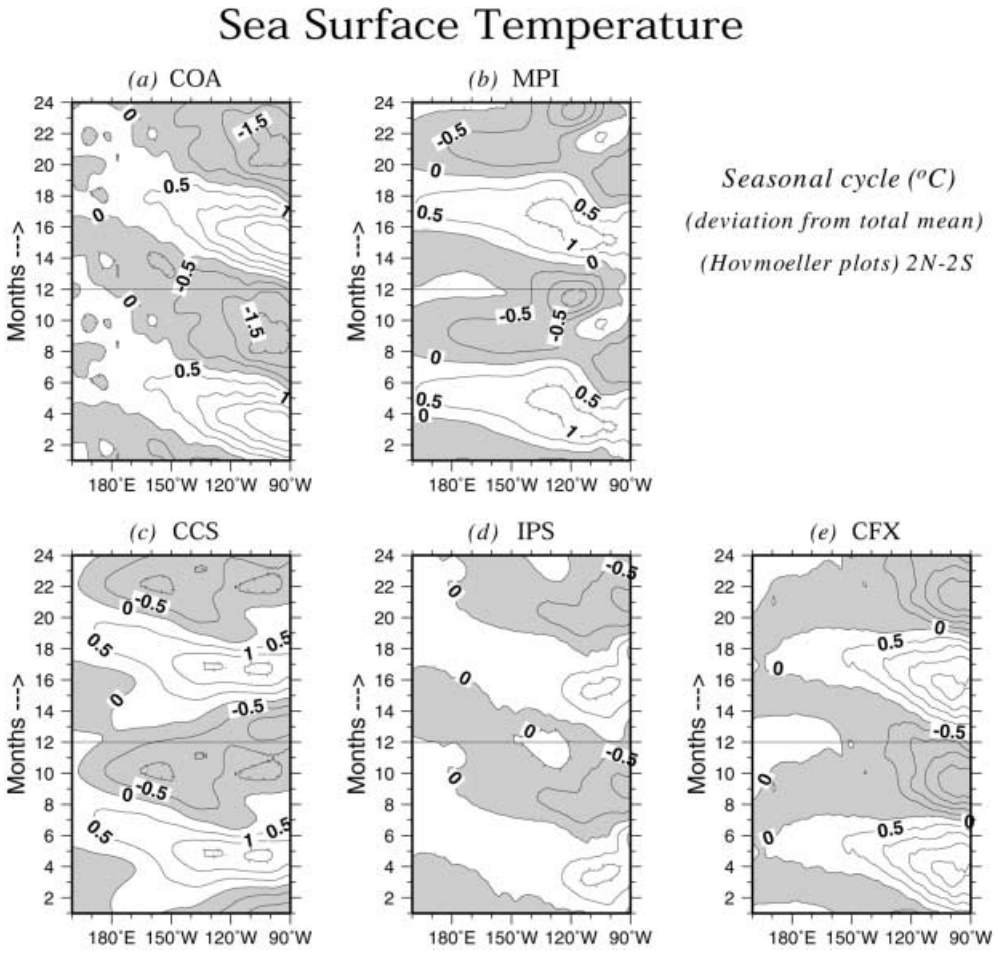

Fig. 2 Sea surface temperature: twice seasonal cycle averaged 2°S–2°N in the deviation from the total mean (units: °C – negative values are *shaded*)

project CoPIVEP (Coupled Processes and Interannual Variability in the Equatorial Pacific). The goal of CoPIVEP is to prospect the eventual link between the mean state or the seasonal cycle and the nature of the interannual variability. The present work shows the results obtained with four coupled models.

The interannual variability will be described through simple statistical analysis of SST and 100 meters temperature anomalies: total variance and empirical orthogonal functions (EOF). The study takes also into account previous work about the definition of possible coupled processes which could be involved in El Niño-like events (Pontaud and Thual 1998, hereafter PT98). In a very simplified formulation of the coupled processes in the equatorial region, PT98 have obtained an explicit formulation of four dynamical processes (named Tx, Tz, Th and W, see Appendix 1) which control the growth rate of an equatorial coupled mode (TK-mode). The efficiency of the four processes and the resulting growth rates are controlled by the annual mean state or the seasonal cycle. Each process is associated with a specific aspect of the basic state: Tx to the zonal gradient of SST, Tz to the vertical gradient of temperature in the ocean, W to the equatorial upwelling and Th to a combination of the upwelling and the vertical gradient of temperature. Then, the annual mean state and the seasonal cycle can be characterised by the intensity of these four different dynamical processes and by the resulting total instability. In this approach, the atmospheric physics are not taken into account and this is certainly a wide point of the study. Moreover, the diagnostics are sensitive to the tuning of some parameters (see PT98).

The coupled models are described in Sect. 2 together with the observations used. Section 3 is devoted to the annual mean state and the seasonal cycle, while Sect. 4 deals with the interannual variability. The coupled processes approach is treated in Sect. 5 (the processes are described in Appendix 1). A discussion of the majors results and conclusions are presented in Sect. 6.

All contributors are listed as authors. The first two and the fourth authors have assembled the model results. The lead author has written the text. Any error or omission remain the responsibility of the lead author.

2 The coupled models

An acronym is given to each of the simulations: MPI for the Max-Planck-Institute, CCS for the Center for Climate System Research, IPS for the Institut Pierre Simon Laplace and CFX for CERFACS. A brief description of each of the models is given in Table 1, together with a reference where details of the respective models can be found. Regarding the atmospheric components (AGCM), three

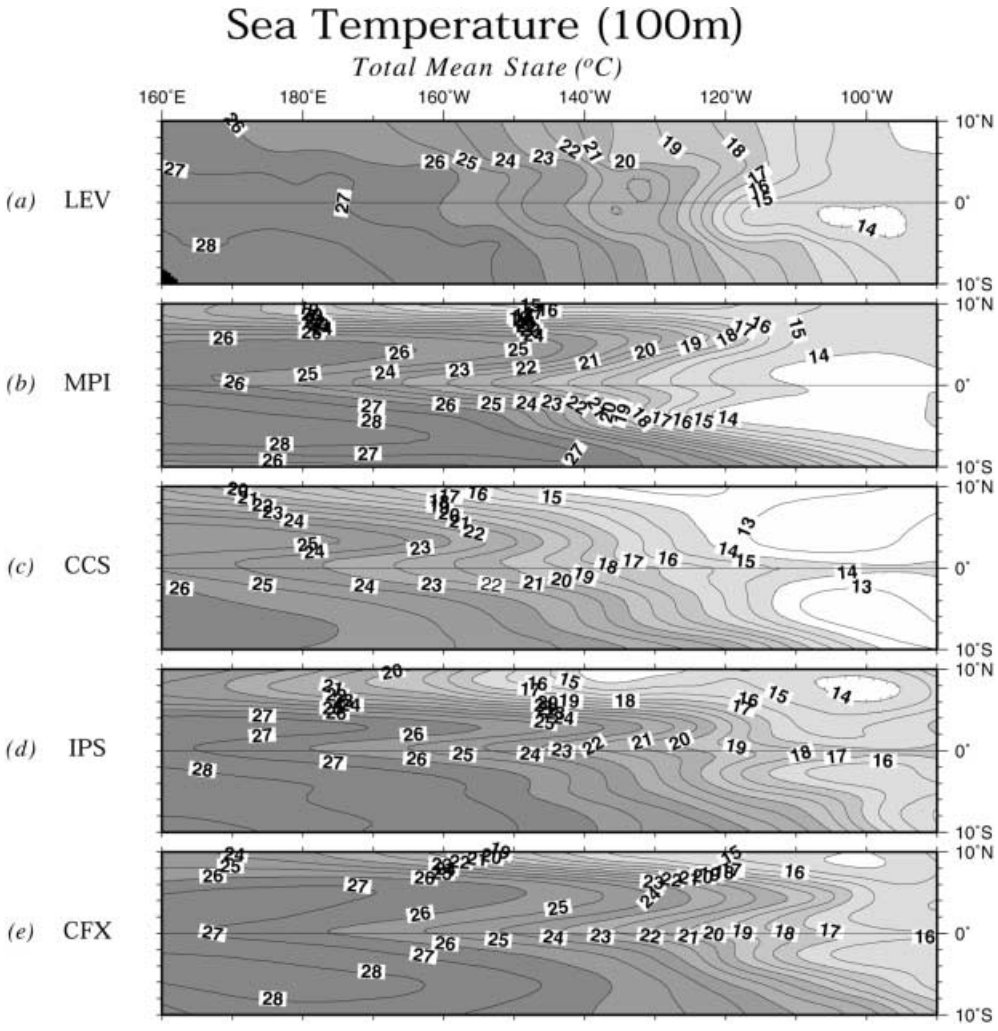

Fig. 3 Sea temperature 100 m: total mean value (units: °C)

are spectral and one (IPS) is a gridpoint model; none of the coupled models shares a common atmospheric component. Horizontal resolution ranges from T21 to T42 and a grid size of about 3° is used in the IPS model. A specific point of IPS is the "delocalised" atmospheric physics which is computed on the oceanic grid (Vintzileos and Sadourny 1997).

The OPA oceanic model of LODYC is used identically in two CGCMs in its Pacific version (Dandin 1993; Stockdale et al. 1993). The two other oceanic models are quasi-global with enhanced horizontal resolution in the equatorial region. Three different mixing parametrisations are used: a Richardson number-dependent scheme with a crude mixed layer scheme and two turbulent kinetic energy schemes with a closure 1.5 and 2.5.

The main dataset for verification is COADS (Comprehensive Ocean-Atmosphere Data Set, Da Silva and Young 1994) referred to as COA. The SST of COA are depicted on a $1° \times 1°$ grid from January 1945 to December 1989. The other datasets come from CAC (Reynolds 1988, hereafter CAC) and Levitus (1982, hereafter LEV). The annual mean and seasonal cycle of the Levitus set are used, because the T100 m is included in this dataset.

3 Mean state and seasonal cycle

3.1 Annual-mean SST

Figure 1 illustrates the annual-mean SST based on COA together with the model simulations. In all the models, the cold tongue is too sharp, mainly in CFX and IPS which have the highest meridional oceanic resolution in the tropics. The core of the cold tongue is shifted too far to the west, mainly in MPI and CCS. The extent of the warm pool is too small in all models.

3.2 The seasonal cycle of equatorial SST

Figure 2 shows the SST seasonal cycle as the deviation from the annual mean for COA and each model simulation. The variation in observed (COA) SST is dominated by the annual harmonic which is strongest in the eastern part of the basin. The warm extreme (+2 °C) in April is stronger than the cold extreme (−1.5 °C) in September–October.

Simulated SSTs are dominated by an annual harmonic in all models. The strongest seasonal variations in equatorial SST are located in the eastern Pacific in all models, although cold deviations can extend into the western part of the basin (MPI and CCS). The seasonal cycle is very weak in IPS but improved relative to M95. Only the CFX simulation captures the relative amplitude and phase of the seasonal cycle. CFX captures

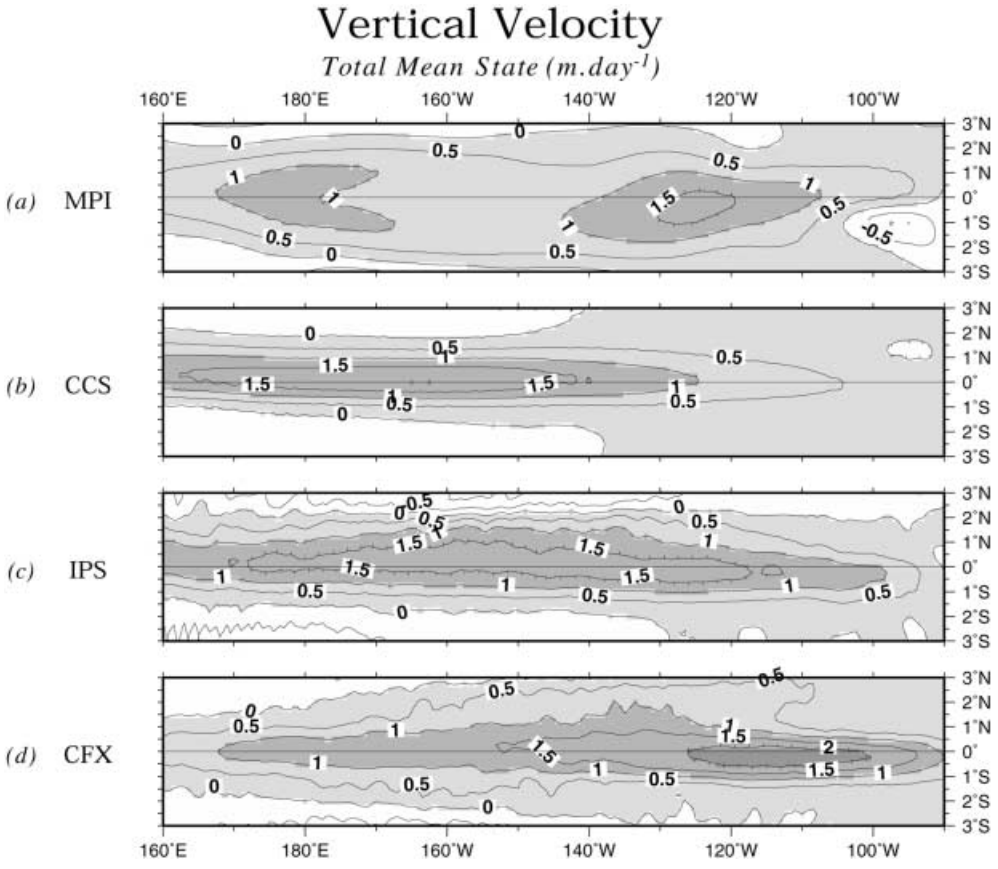

Fig. 4 Upwelling: total mean value (units: m day^{-1})

again quite well the westward propagation of the seasonal maxima and transitions.

3.3 Annual mean T100 m

The sub-surface temperature determines partly the vertical gradient which occurs in the processes *Tz* and *Th*. It will be studied through the temperature at about 100 m (see Fig. 3). The annual mean of the Levitus (LEV) data set is used as a reference. The field of 100 m temperature shows the cold water in the eastern part of the basin with a westward extension along the equator. This ''deep cold tongue'' is very sharp and extends too far westward in all the models. The cold water in the east is too warm in the CFX and IPS models which used the same oceanic component OPA and thus the same turbulent mixing scheme (TKE 1.5).

3.4 Annual mean upwelling

Figure 4 shows the annual mean upwelling (between 3°S and 3°N). It is an average from the surface to about 100 m depth for all the models except MPI: the mean upwelling of MPI is shown at the only available model level 87 m. The CFX and IPS models simulate a different upwelling structure despite the same oceanic component. The core of the CFX upwelling is located in the eastern part of the basin. The IPS upwelling spreads over the whole basin while the CCS's one is shifted to the western and central parts of the basin. The structure of the MPI upwelling shows two cores, one in the eastern part and one in the western part with a downwelling in the eastern part of the basin. It should be noted that the oceanic features do not necessarily reflect properties of the ocean components, but also properties of the atmospheric models which determine partly the ocean state through the surface wind stresses and heat fluxes.

4 Description of the interannual variability

The interannual variability will be essentially described through the SST in terms of simulated variance and principal component analysis. The interannual signal of SST have been defined month by month as the deviation from the mean seasonal cycle.

4.1 Total variance

Figure 5 illustrates the spatial structure of the total variance of the interannual SST variability. Most models produce a maximum variance in the eastern part of the basin along the equator and miss the relative maximum in the central Pacific (see COA). The simulated

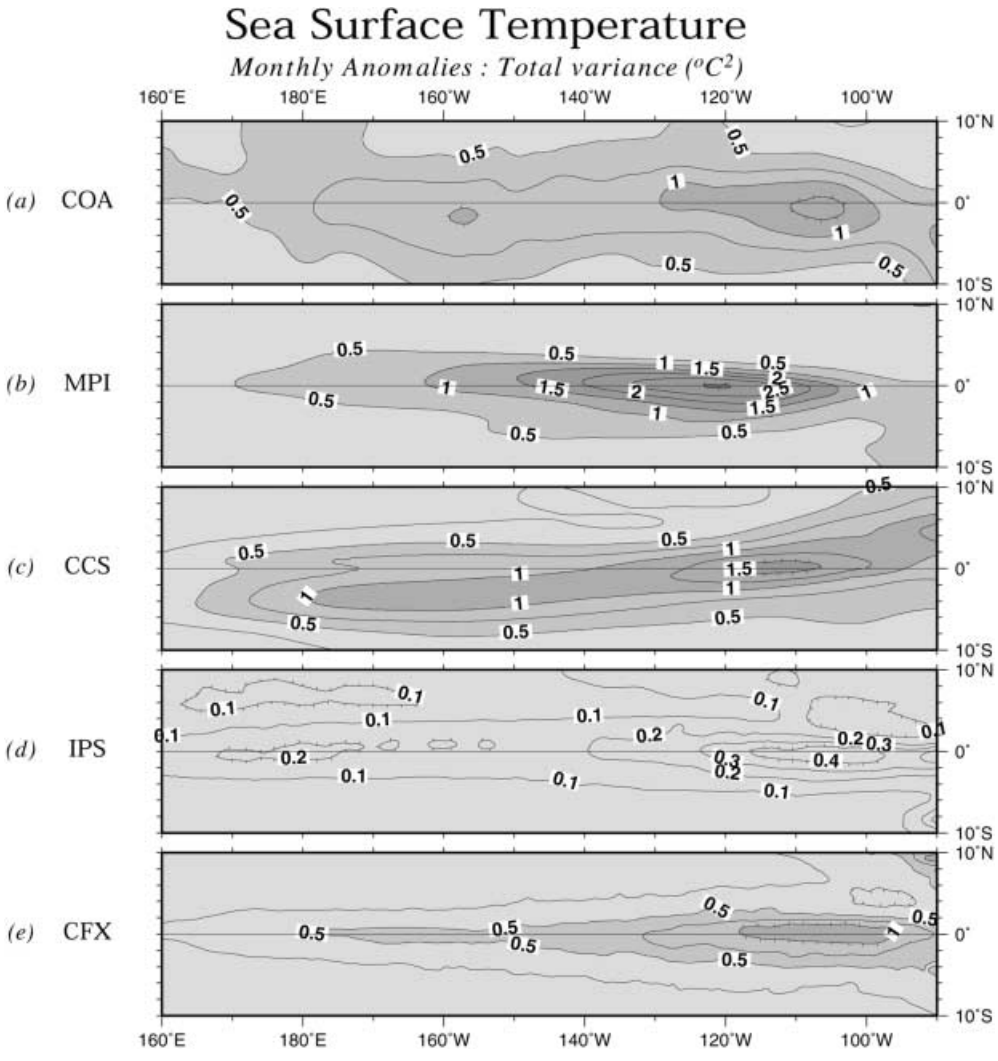

Fig. 5 Total variance for the monthly anomalies of SST (units: $°C^2$)

structures are generally too sharp in the north-south direction. The structure simulated in CCS shows an orientation west-southwest/east-northeast: the interannual signals evolve mainly along this axis. At subsurface level (T100 m), all the models show a symmetric structure along the equator consistent with Kelvin or Rossby 1 structure (not shown).

4.2 Seasonal cycle of the total variance deviation

Figure 6 shows the seasonal fluctuation of the variance of the SST anomalies. From the observations (COA), the maximum variance occurs in December. The MPI, CCS and CFX simulations show a significant seasonal change of the total variance, indicating a phase locking of the interannual variability to the seasonal cycle. The IPS simulation shows a weak 6-month modulation in the eastern part of the basin. In the CCS simulation, the maximum variance occurs during the cold phase of the SST seasonal cycle (Fig. 2); the precise maximum occurs in January–February which is also the time when the seasonal cycle minimum is reached in the eastern Pacific. IPS has two seasonal maxima of variance: one with the warm phase and one with the cold phase of the SST seasonal cycle. In MPI, the total variance evolves with the warm-to-cold transition and reaches its maximum with the colder phase. The seasonal variation of the variance simulated in CFX is realistic, but the maximum occurs one month too late in January.

4.3 Empirical orthogonal functions

An empirical orthogonal function (EOF) analysis has been performed using the covariances (and not the correlations), which emphasises the areas with large variations. The eigenvector of each EOF is normalised to unity. The EOF analysis has been computed for the area 160°E–90°W and 10°S–10°N. Figure 7 shows the spatial structures of the first SST EOFs. Overall the SST EOFs are very similar the variance plots shown in Fig. 5. All models simulate a too narrow structure along the equator and miss the western maximum of COA. The CCS pattern again shows the WSW to ENE orientation. (This point is consistent with the apparent propagation

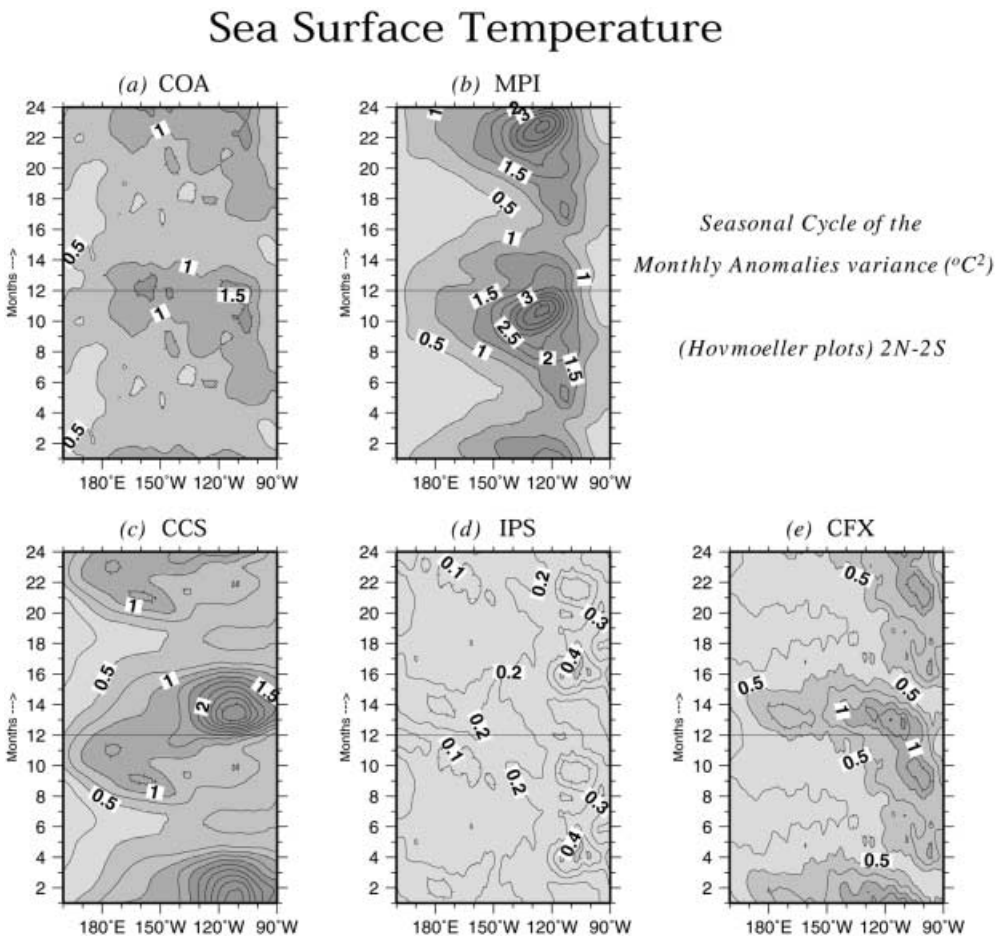

Fig. 6 Seasonal cycle of averaged 2°S–2°N variance for the monthly anomalies of SST (units: $°C^2$)

(computer frames animation) of the interannual signals along this axis.) IPS and CFX have very similar EOFs. An explanation could be the common oceanic component OPA which may define the spatial structure of the first SST EOF through the resolution and/or the parametrisations. However, it should be remembered that the atmospheric components are quite different, so that it remains surprising that the SST EOFs are so similar.

Figure 8 shows the spatial structures associated with the second SST EOFs. All models simulate an east-west dipole consistent with COA. The structures are generally too narrow.

Figure 9 shows the spatial structures associated with the first T100 m EOF. The MPI, CCS and IPS models share a quite similar structure which is reminiscent of an equatorial Rossby wave pattern, while CFX has a Kelvin-like structure. It has been noted already that CFX and IPS have a similar first SST EOF. A possible argument was the common oceanic model, but this argument fails at subsurface.

4.4 Inter-EOF relations

Figures 10 and 11 show that the three EOFs (1st and 2nd SST and 1st T100 m) have the same dominant frequency for each model. This suggests a possible link between each of the EOFs. In contrast, the first and second SST EOF of COA do not exhibit the same dominant frequency. (The length of the data sets are: COADS = 45 years, MPI = 20 years, CCS = 65 years, CFX = 20 years, IPS = 29 years.)

SST-EOF1 versus SST-EOF2

Figure 12 shows the lag-correlation between the first and the second SST EOF. The left column depicts how the second EOF follows the first and the right column how the first EOF follows the second. The lag-correlations are weak but larger in the left column (around 0.5 for the models). This indicates that the second EOF tends to follow the first EOF by a few months. All the models indicate that the second EOF would follow the first EOF with the reverse sign, while it is the opposite in COA (remembering the weakness of the lag-correlation in COA). Then, in COA, the second SST EOF could be associated with an increasing warming in the eastern Pacific and a cooling of the warm pool after the onset of an El Niño while the second EOF of the models could be associated rather with the normal state return than with a prior build-up phase. Moreover, the second SST EOFs of the C-GCMs are quite similar independent of the structure of the first EOFs. This could indicate that the

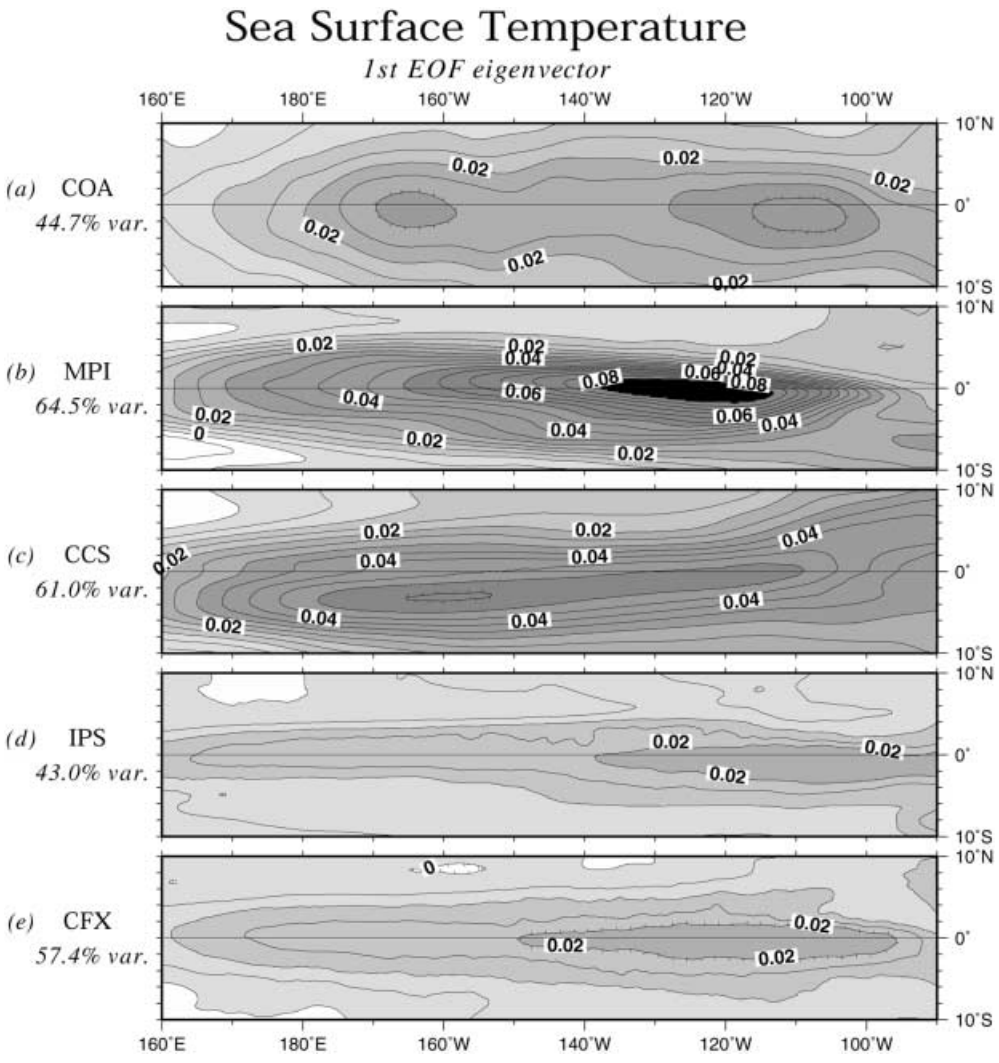

Fig. 7 Eigenvector of the 1st EOF for the monthly anomalies of SST

all models use the same method to return towards the normal state, through a common dynamics concentrated along the equator.

SST-EOF1 versus T100 m-EOF1

Figure 13 shows the lag-correlation between the first SST and T100 m EOFs. The lag-correlations are larger than those of Fig. 12. This indicates a stronger link between the surface and subsurface first EOFs. In CFX, there is no lag between the two EOFs. In contrast, in the IPS model (with the same ocean component) the first SST EOF follows the first T100 m EOF by three months. In IPS, the source of the variability comes from the perturbations of the ITCZ location (Vintzileos et al. 1999b). These perturbations force anomalies in the ocean around 5°/10°N which travel equatorward at subsurface levels. The interannual signals appear first in the equatorial thermocline and upwell to the surface. In CFX model the surface and the subsurface temperature vary in phase and have very similar patterns. The interannual signals and the associated anomalies would be linked and homogeneous along the vertical. MPI and IPS share similar eigenvectors but the delay is shorter (one or two months) and the lag-correlation larger. Whatever the source, the interannual signals of MPI seem also to propagate from the subsurface to surface but more rapidly than in IPS. However, the mean upwellings are similar in the areas concerned. It is difficult to involve either the different vertical mixing schemes or the vertical discretisation or the numerical schemes of the vertical advection or the probable different dynamics of the interannual variability. In contrast, CCS shows that the first T100 m EOF would follow the first SST EOF by six months. This indicates a different dynamics of the interannual signals where the surface would drive the subsurface.

5 The coupled processes approach

5.1 Process descriptions

The mean state can be described through the intensity of the processes Tx, Tz, Th and W (keeping in mind the

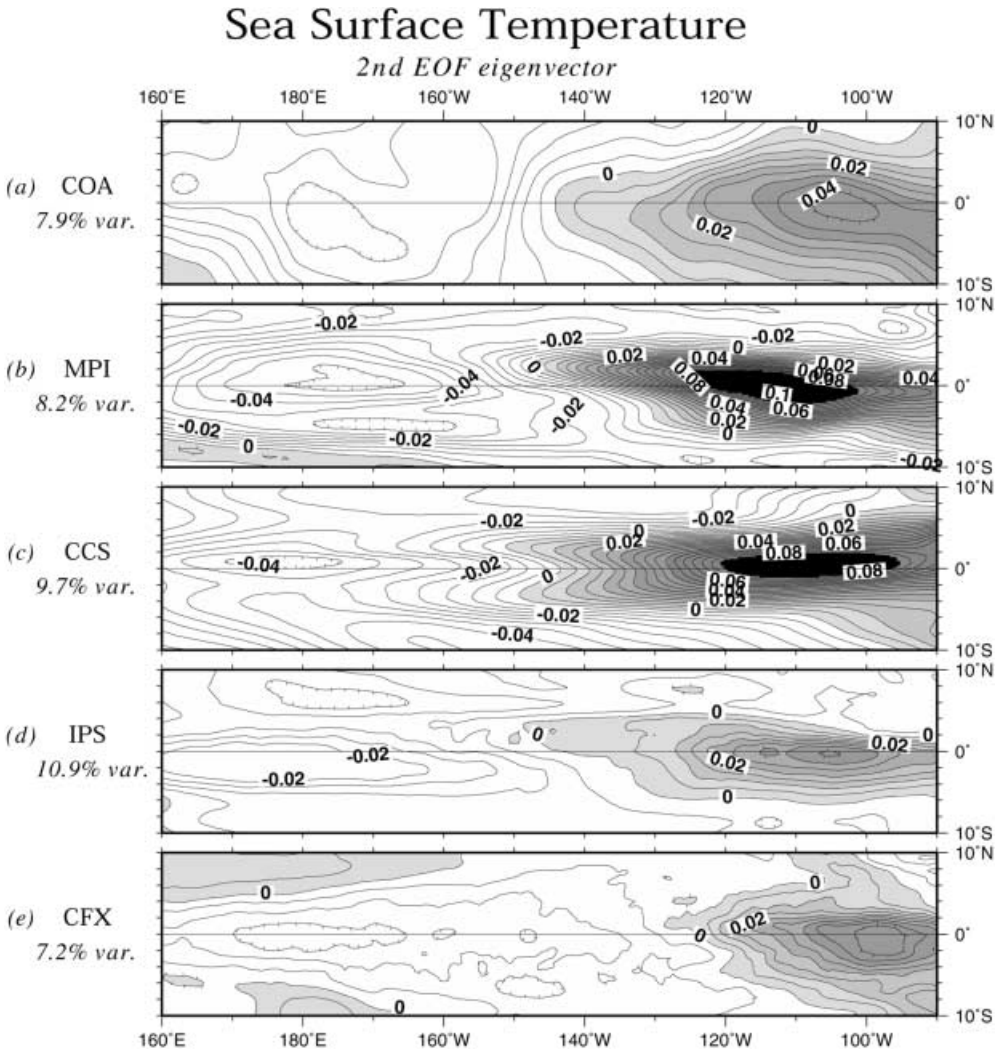

Fig. 8 Eigenvector of the 2nd EOF for the monthly anomalies of SST

simplicity of the PT98 work). The physics and the analytical formulation of the processes are briefly outlined in Appendix 1. Table 2 shows for the all models the intensity of each of the processes and (when it is possible) for observations (COA, LEV and CAC). The processes have been computed in the Nino3 + Nino4 box, i.e. the area 160°E–90°W and 5°S–5°N.

The *Tx* process is proportional to the zonal gradient of SST. COA and CAC are in agreement while LEV overestimates its intensity. Despite the cold bias and the narrow structure of the SST field, CFX fits well the zonal SST gradient. The other models underestimate the difference of SST between the two sides of the basin: the eastern cooling is too weak in IPS and slightly shifted westward in MPI and CCS. In these two simulations, the zonal gradient of SST is reversed in the eastern part.

The absolute value of the *W* process is proportional to the mean upwelling. CFX and IPS, which share the same oceanic component OPA, have an average upwelling with comparable intensity (but with a different structure, see Fig. 4). MPI and CCS have also a comparable averaged upwelling which is weaker. The *Tz* process is proportional to the vertical gradient of temperature (between the surface and 100 m depth). IPS is close to LEV, while the vertical gradient of CFX is weaker, despite the comparable averaged upwelling. Again, MPI and CCS, with a comparable averaged upwelling, simulate different vertical gradients. The upwelling alone should be insufficient to explain the vertical structure of temperature.

From the coupled processes point of view, the interannual variability is driven mainly:

1. By the zonal SST gradient (*Tx*) in CFX (i.e. with zonal current anomalies)
2. By the vertical gradient (*Tz*) in CCS (i.e. with the upwelling anomalies)
3. By vertical and zonal gradients of temperature in MPI and to a lesser extent in IPS.

These results cannot be derived from the variance and EOF analysis. The thermocline effect is weak in all the simulations. However, the weakness of the thermocline process *Th* can be directly linked to the

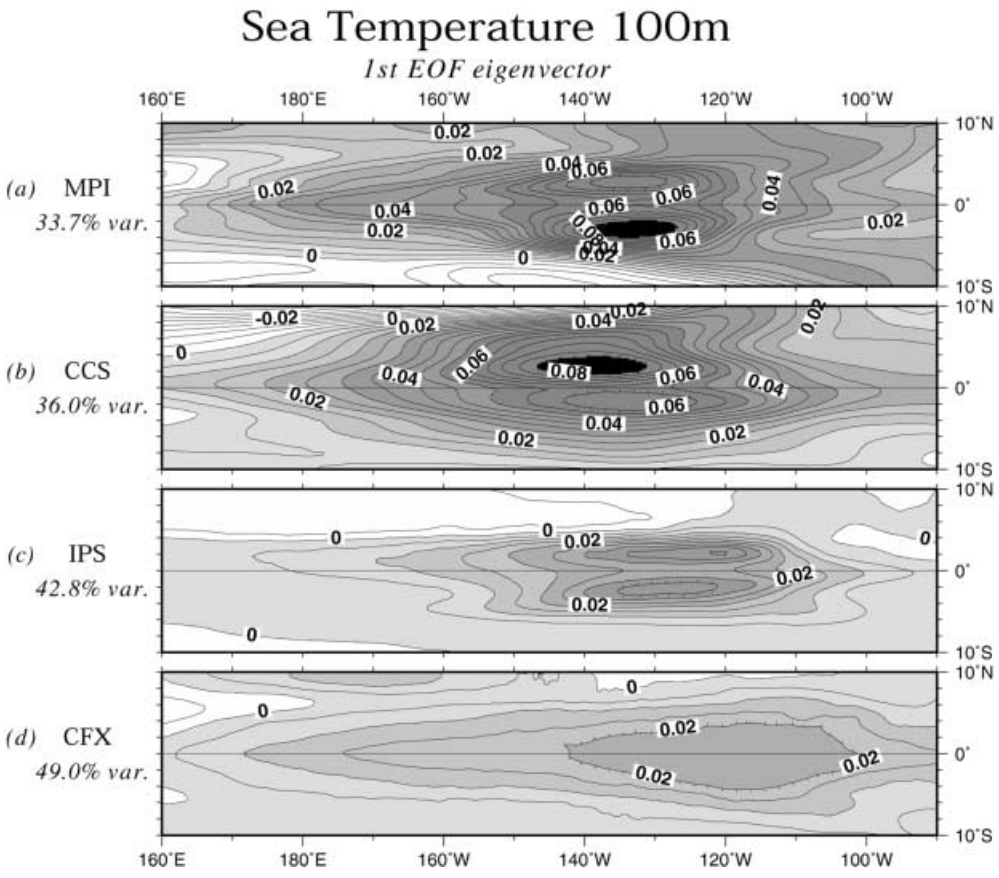

Fig. 9 Eigenvector of the 1st EOF for the monthly anomalies of T100 m

simplified approach of PT98 which underestimates this process.

5.2 A "total mean" link ?

Table 2 shows also, for the all models, the local extremum and the average of the variance and the growth rate. The average of the total variance has been computed on the area 160°E–90°W and 10°S–10°N. The extremum of the variance is considered an indicator of the intensity of the interannual variability. The extremum of variance increases with the total growth rate. The more unstable the mean state is, the higher the interannual signals are. In contrast, no clear link appears between the growth rate and the averaged variance. The basic state, described through the total growth rate would controls the extremum of the interannual variability but not its spatially averaged intensity.

5.3 A "seasonal" link ?

The question posed frequently is the role of the seasonal phase locking of ENSO. Figure 14 shows that the total growth rate is strongest a few months before the maximum of variance in MPI and CFX. This may reinforce the idea that the seasonal cycle controls the life cycle of ENSO. However, this link does not appear in CCS and IPS. In CCS, the total growth rate remains constant over the seasonal cycle: this results from a balance between the seasonal opposition of Tx and Tz. In IPS, there is a seasonal variation of the total growth rate but no significant impact on the interannual variability. The possible role of the seasonal cycle in MPI and CFX is consistent with the dominant frequencies of the EOFs which are multiples of 12 months.

6 Discussion and conclusion

The interannual signals over the tropical regions and a possible link with the annual mean state and the seasonal cycle have been examined in four coupled GCMs.

The spatial structure of the interannual variability is too narrow. Perhaps the models spuriously excite some higher ocean vertical modes which have a sharper meridional structure. Adding the second and the third baroclinic modes in a Zebiak and Cane like-model concentrates the interannual signals along the equator (personal communication Dewitte). In the subproject DIVCOP of CMIP (Pontaud et al. 1998), the oceanic GCM meridional resolution is cruder than it is in the present study and the meridional structure of the interannual signals is larger. These points suggest that the higher the meridional resolution, the sharper the interannual signals are.

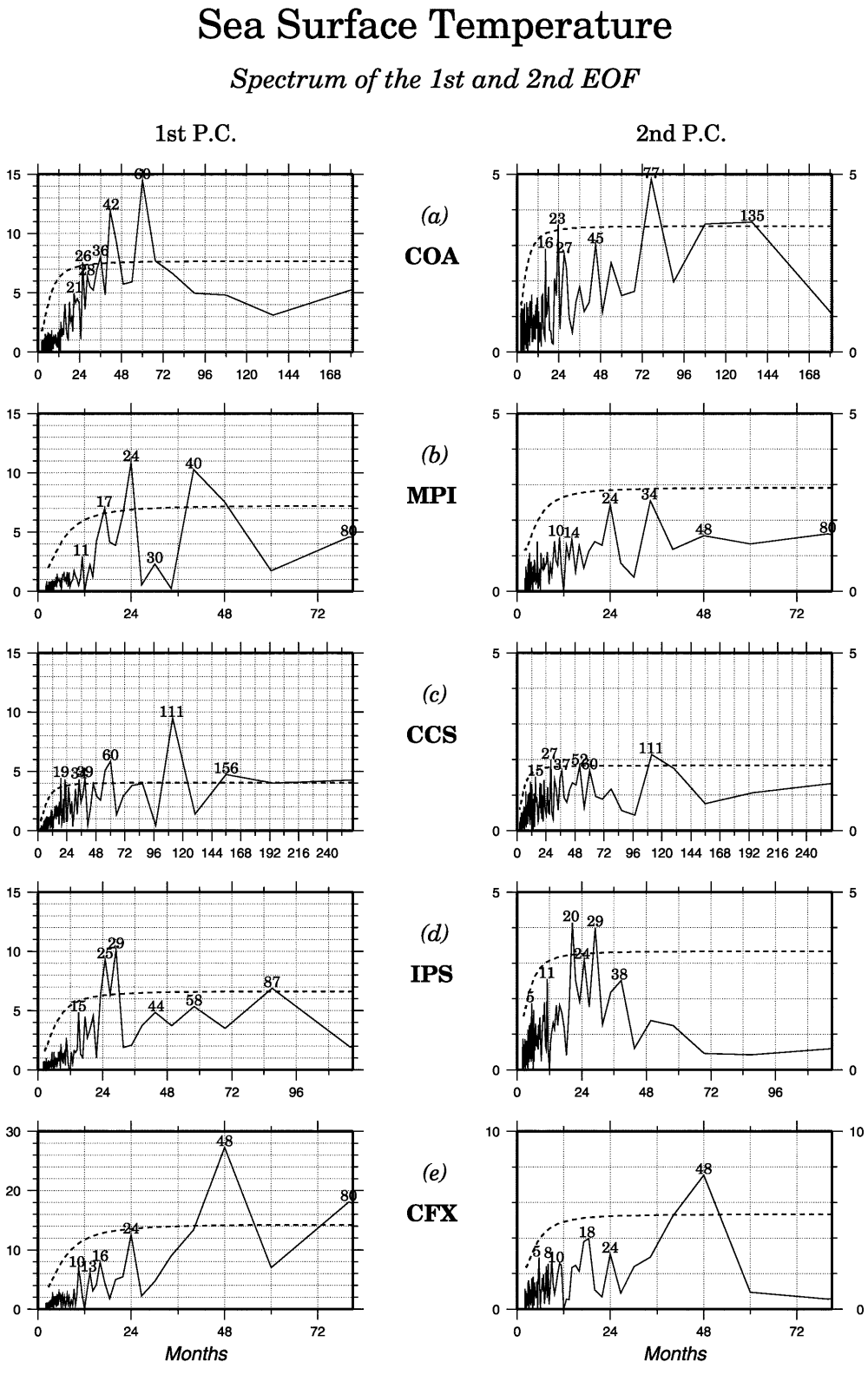

Fig. 10 Spectrum of the first and second EOF of the SST (*dotted line* is 95% confidence level)

The structures of the anomalies in IPS and CFX, which share the same oceanic model, suggest that the oceanic model would control the surface structure of the interannual signals despite the different atmospheric models. In constrast, the atmospheric models trigger different mechanisms in the ocean with different signatures in depth.

The lag-correlation between the first SST EOF and the first T100 m EOF are similar in IPS and MPI (the information would propagate from the subsur-

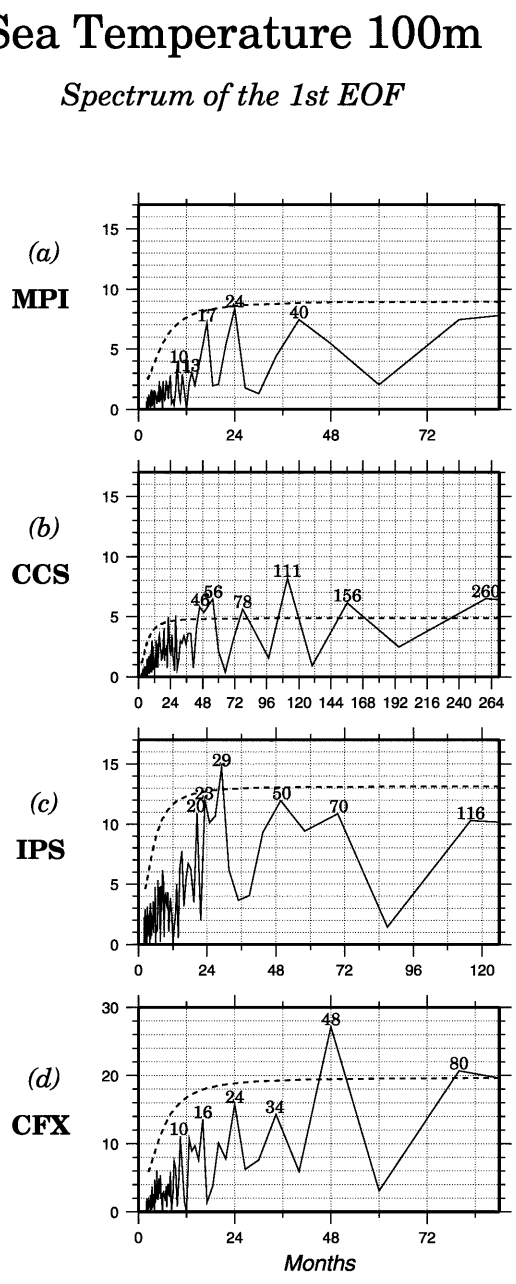

Fig. 11 Spectrum of the first T100 m EOF (*dotted line* is 95% confidence level)

face towards the surface). In these two simulations, the *Tz* and *Tx* processes are involved quite equally. CFX, which favours the *Tx* process, has simultaneous anomalies in the surface and subsurface, while CCS, which favours the *Tz* process, simulates the anomalies at first in the surface and then six months later in the subsurface. It is difficult to find a dynamical link between the surface-subsurface connection and the basic state. The simplest explanation could be found in the atmospheric component. The source of the IPS interannual variability comes from the ITCZ location anomalies. One can notice that the IPS coupled model computes the atmospheric physics on the oceanic grid. Then the atmospheric fluxes have the same high resolution as the ocean dynamics. This could favour the specific coupling between the ITCZ and the ocean dynamics.

In each model, the three studied EOFs (1st and 2nd SST and 1st T100 m) show the same common dominant frequency while this is not the case in COA. Two models develop clearly a dominant frequency multiple of 12 months. These two models also show a significant seasonal modulation of the anomaly variance. Their interannual signals seems to be influenced by the seasonal cycle in agreement with the seasonal variation of the total growth rate. Their total growth rates present a maximum a few months before the maximum of the anomalies variances. The maximum instabilities occur in summer or fall. In contrast, IPS, which has a significant but weaker seasonal modulation of the total growth rate, does not simulate such a modulation of the anomalies variance. Overall, the IPS variance is weak. It seems that IPS does not reach a sufficient level of instability to develop significant interannual variability, while MPI and CFX would go beyond this level. This remark would indicate that the mean state (annual and seasonal cycle) plays a role in the characteristics of the interannual variability.

In MPI and CFX, the interannual variability is confined with in the equatorial wave guide and then can be driven by the 12-month seasonal cycle and amplified by the local positive feed-back. That can explain the dominant 24 or 48 month frequencies. The specific coupling involved in the IPS interannual signals (through the ITCZ location) is not solely driven by the equatorial dynamics even if equatorial coupled processes may contribute to the growth. It may be noticed that the dominant frequency is not associated with the annual cycle. Another behaviour is simulated by CCS: the anomalies variance shows a seasonal modulation while the total growth rate is quite constant over the year. In CCS, the maximum anomaly variance does not show an evident link with any component of the equatorial seasonal cycle (either the SST, or the upwelling). One is reminded that the CCS SST interannual signals slip out of the equator and are dominated by the very low frequency 111 months. Thus, the dominant frequencies would depend on where the interannual anomalies occurs and which specific coupling develops.

Keeping in mind the extremely few coupled models considered, a possible link appears between the mean state and the intensity of the interannual variability. The greater the degree of instability of the mean state, the more severe the signals. The local growth rate through coupled processes would control the intensity whatever the source of the interannual variability can be. The annual cycle, if significant, would control the phase locking. The dominant frequency would depend on the location of the anomalies: when confined along the equator and free of off-equatorial triggering, the dominant frequency is a 12-month multiple.

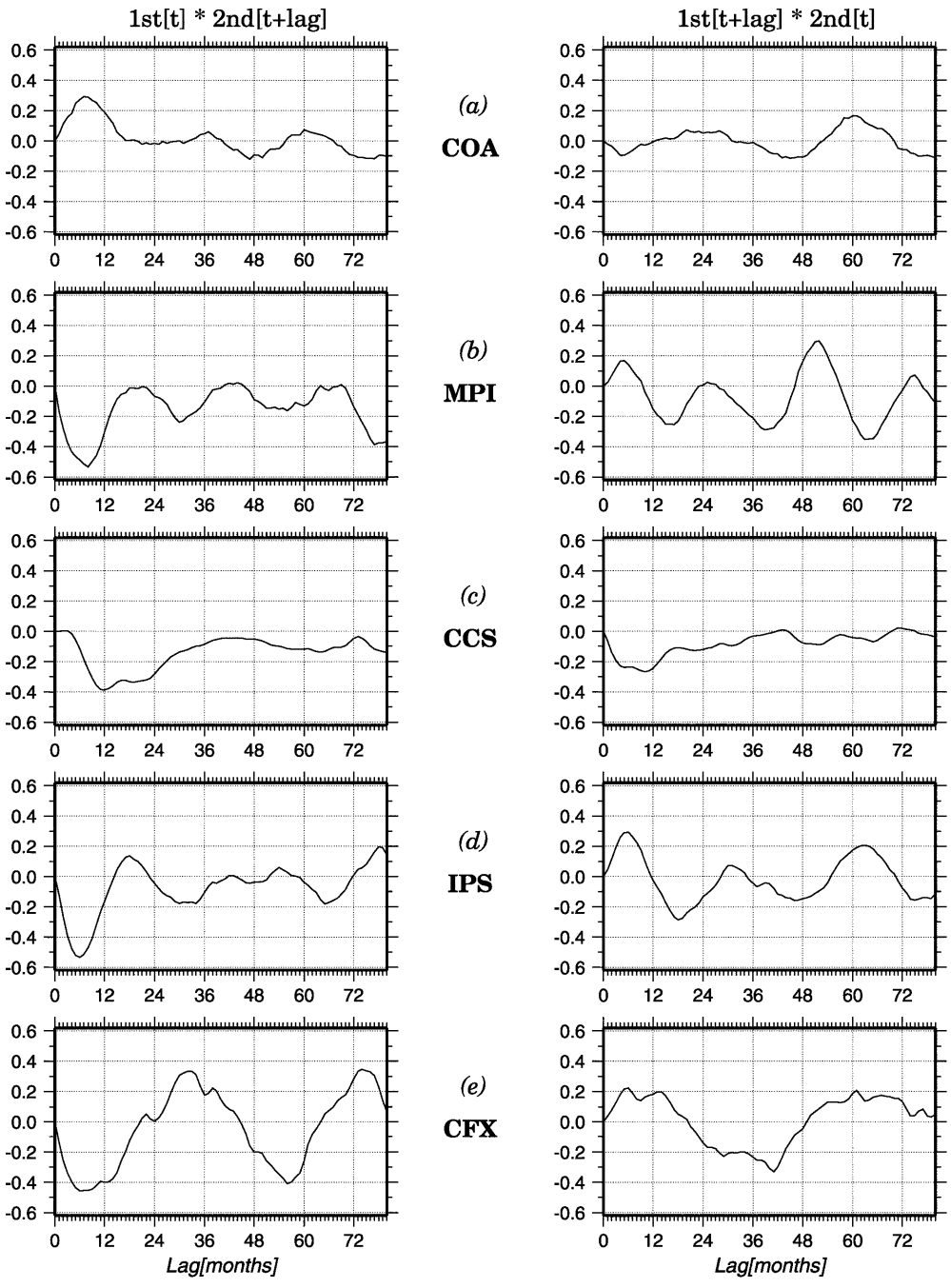

Fig. 12 Lag-correlation between the first and second SST EOF

The second SST EOF of all the models are quite similar and would correspond to the return to the normal state while the one of the observations would favour the initial anomaly. The models are apparently unable to maintain the anomalies correctly. While the first EOFs are different between the coupled models, the second one is more similar. It would seem that all the coupled GCM use the same way to return towards the normal state. The structures are quite confined along the equator. This suggests that the return to the normal state is made through equatorial dynamics which sounds like an oceanic wave adjustment.

It has been mentioned that the type of coupling, which dominated during a simulation, would be of prime importance in the seasonal phase lock. Then it is important to determine the nature of the interan-

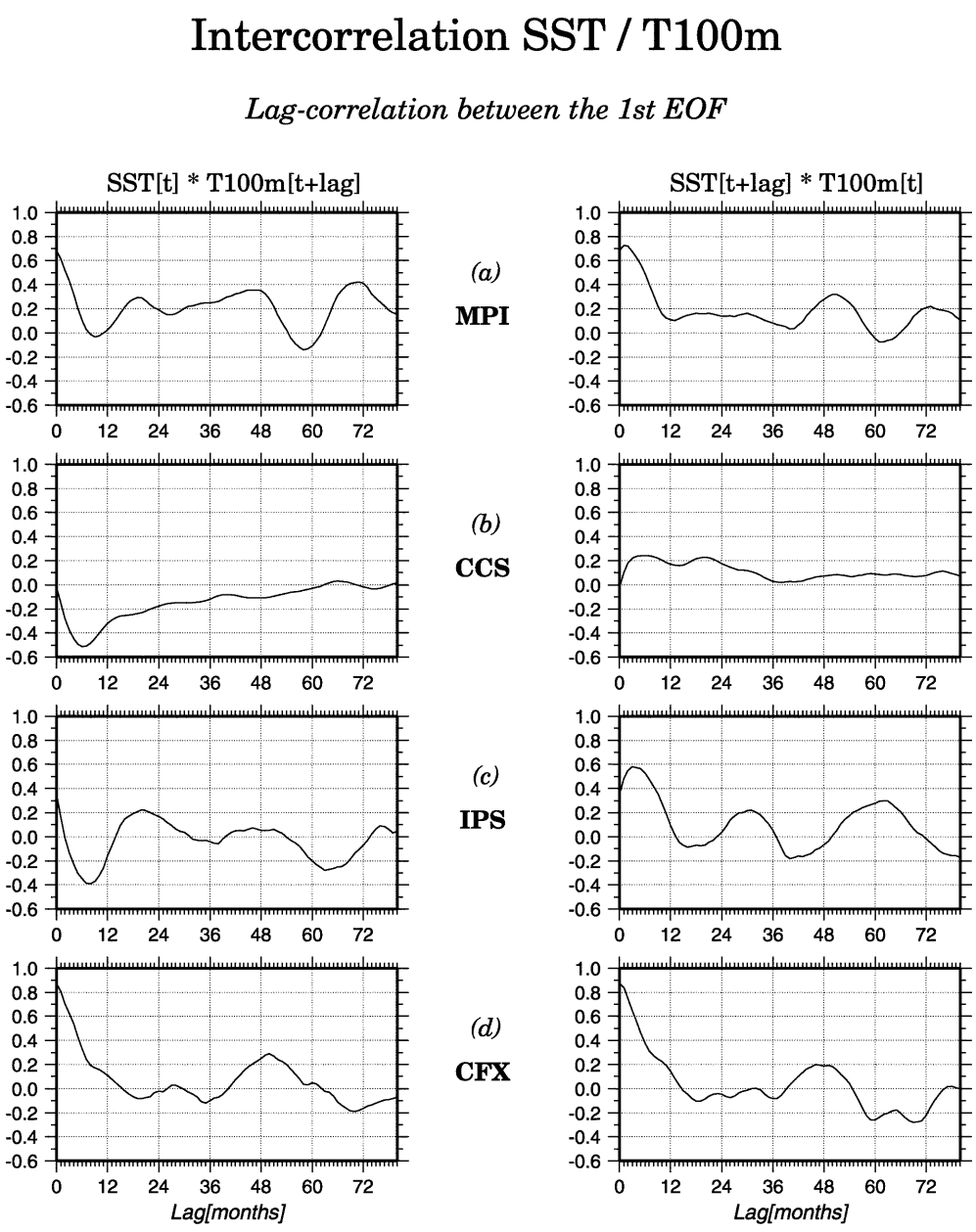

Fig. 13 Lag-correlation between the first EOF of SST and T100 m

Table 2 SST total variance: the maximum value and the average in the (160°E–90°W × 10°S–10°N) box (unit: °C^2); the growth rate and the processes *Tz*, *Tx*, *Th* and *W* (unit: 10^{-3} day^{-1}): total mean value

Models	Variance maximum (°C × °C)	Variance average (°C × °C)	Growth rate 10^{-3} days^{-1}	*Tz* 10^{-3} days^{-1}	*Tx* 10^{-3} days^{-1}	*Th* 10^{-3} days^{-1}	*W* 10^{-3} days^{-1}
MPI	3.04	0.50	6.298	3.721	3.717	0.676	−1.816
CCS	1.59	0.58	5.313	4.831	1.473	0.926	−1.917
CFX	1.31	0.36	5.048	2.036	5.285	0.581	−2.854
IPS	0.50	0.14	4.344	2.950	3.427	0.850	−2.883
COA	1.30	0.65			4.892		
CAC					4.803		
LEV				3.156	6.360		

nual signals. Previous theoretical works (Hirst 1986; Neelin 1991; PT98) may be a guide. To reach this goal, basic requirements would be the interannual data (not available in this analysis) of the oceanic temperature, zonal current and surface wind stress, and possibly the surface pressure, thermocline depth and upwelling. Such information is difficult to include in an intercomparison. A common protocol should be defined to achieve this analysis in each laboratory concerned.

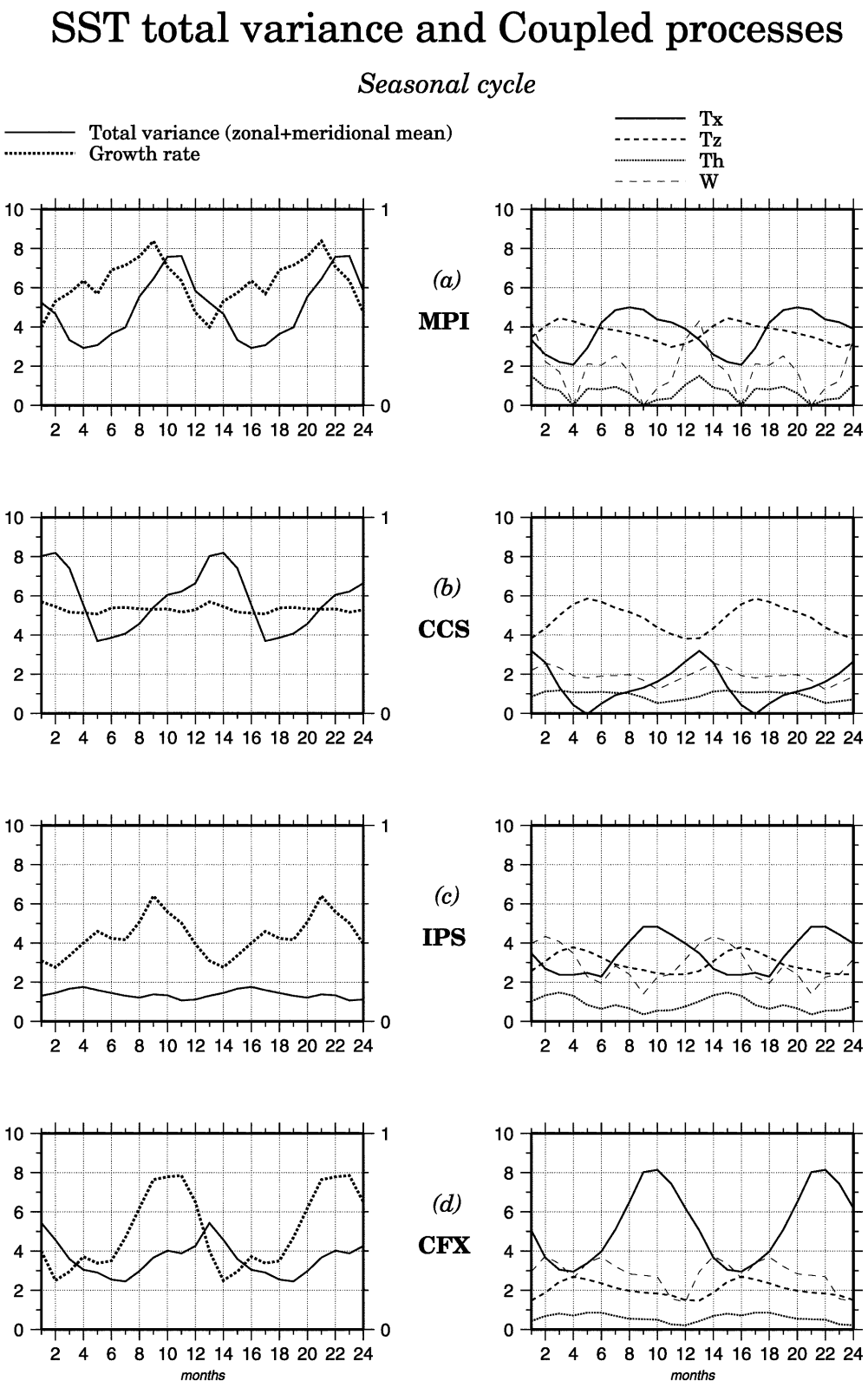

Fig. 14 Seasonal variation of: (*left*) total variance and growth rate; (*right*) *Tx*, *Tz*, *Th* and absolute value of *W*. Units: total variance in $°C^2$; growth rate and processes in 10^{-3} day^{-1}

Acknowledgements The lead author thanks P. Delecluse, C.R. Mechoso and S.G.H. Philander for supporting the initiation of the CoPIVEP project and M. Latif for his contribution to this work. The author Augustin Vintzileos wishes to mention that his work was supported by the European Union under Contracts EV5V-CT92-0121 and ENV4-CT95-0109 and the PNEDC. Numerical experiments have been conducted at IDRIS (Institut de Développement et de Recherches en Informatique Scientifique) of the CNRS. Plots have been made with the GMT software.

Appendix 1

The coupling of an oceanic shear layer and an oceanic equatorial Kelvin wave with a simple atmospheric model has given a full explicit formulation of a coupled mode (PT98). This mode could be a simplification of El Niño-like events. Its amplitude is controlled by the four dynamical processes:

1. The Tx process is based on the advection of the mean zonal gradient of SST by the zonal current anomaly. A positive (negative) current induces a surface warming (cooling) which controls a wind stress anomaly that reinforces the positive (negative) zonal current and then the warming (cooling). The feed-back is positive.

2. The Tz process is based on the advection of the mean vertical gradient by the vertical velocity anomaly. A positive (negative) vertical velocity anomaly induces a surface cooling (warming) which controls a zonal wind stress divergence (convergence). This wind field favours an oceanic surface divergence (convergence) which increases the positive (negative) vertical velocity anomaly and then the cooling (warming). The feed-back is positive.

3. The Th process is based on the modulation of the mean cooling associated with the mean upwelling by the depth anomaly of the thermocline. A positive thermocline anomaly decreases the vertical gradient of temperature, and then, cooling by the upwelling. That favours a positive SST anomaly which drives a positive wind stress anomaly and then a deepening of the thermocline. The feed-back is positive.

4. The W process is not a coupled one. A positive SST anomaly increases the vertical gradient of temperature and then the cooling by the mean upwelling. The initial warming is damped.

The analytical expressions of the resulting total growth rate and of each process are:

$$GR = \frac{1}{\varepsilon_s}\frac{H_2}{\rho H}\frac{k^2\alpha_c}{1+\lambda^2k^2}\gamma_z - \frac{W_0}{H} - \frac{1}{\rho HC}\frac{\alpha_K}{1+\lambda^2k^2}\gamma_x + \frac{1}{\rho Hc^2}\frac{\alpha_K}{1+\lambda^2k^2}W_0\gamma_z \quad \text{(A1.1)}$$

$$Tx = -\frac{1}{\rho Hc}\frac{\alpha_K}{1+\lambda^2k^2}\gamma_x \quad \text{(A1.2)}$$

$$Tz = -\frac{1}{\varepsilon_s}\frac{H_2}{\rho H}\frac{k^2\alpha_c}{1+\lambda^2k^2}\gamma_z \quad \text{(A1.3)}$$

$$Th = \frac{1}{\rho Hc^2}\frac{\alpha_K}{1+\lambda^2k^2}W_0\gamma_z \quad \text{(A1.4)}$$

$$W = -\frac{W_0}{H} \quad \text{(A1.5)}$$

where γ_x is the zonal gradient of SST, γ_z is the vertical gradient of temperature (between the surface and 100 m depth) and W_0 the equatorial upwelling. These three values are the inputs from the coupled models to perform the diagnostics. The other parameters are defined from the simple oceanic and atmospheric models. The values used are:

$\varepsilon_s = 1.1574074\text{E-}5\ \text{s}^{-1}$
$H = 100.\ \text{m}$
$H_1 = 40.\ \text{m}$
$H_2 = 60.\ \text{m}$
$\rho = 1000.\ \text{kg m}^{-3}$
$k = 5.2359878\text{E-}7\ \text{m}^{-1}$
$\lambda = 2.7009489\text{E}6\ \text{m}$
$c = 2.4\ \text{ms}^{-1}$
$\beta = 2.27\text{E-}11\ \text{m}^{-1}\text{s}^{-1}$

From the diagnostic point of view, the absence of physics (convection for example) in the atmospheric component of PT98 and the simplicity of both ocean and atmosphere dynamics, should be remembered.

References

Dandin P (1993) Variabilité basse fréquence simulée dans l'océan Pacifique tropical. PhD Thesis, Pierre et Marie Curie University, Paris, 300pp

Da Silva AM, Young CC (1994) Atlas of surface marine data 1994. Vols 1–5. Department of Geoscience, University of Wisconsin-Milwaukee, pp 60-416-413-308-416

Frey H, Latif M, Stockdale T (1997) The coupled GCM ECHO-2. Part I: the tropical Pacific. Mon Weather Rev 125: 703–720

Hirst A (1986) Unstable and damped equatorial modes in simple coupled ocean-atmosphere model. J Atmos Sci 43: 606–630

Kimoto M, Yoshikawa I, Ishii M (1997) An ocean data assimilation system for climate monitoring. J Meteorol Soc Japan 75: 471–487

Levitus S (1982) Climatological Atlas of the world ocean. NOAA Prof Pap 13 US Government Printing Office, Washington, DC, USA

Mechoso CR, Robertson AW, Barth N, Davey MK, Delecluse P, Gent PR, Ineson S, Kirtman B, Latif M, Le Treut H, Nagai T, Neelin JD, Philander SGH, Polcher J, Schopf PS, Stockdale T, Suarez MJ, Terray L, Thual O, Tribbia T (1995) The seasonal cycle over the tropical Pacific in general circulation models. Mon Weather Rev 123: 2825–2838

Neelin JD (1991) The slow sea surface temperature mode and the fast-wave limit: analytic theory for tropical interannual oscillation and experiments in a hybrid coupled model. J Atmos Sci 48: 584–606

Neelin JD, Dijkstra HA (1995) Ocean-atmosphere interaction and the tropical climatology. Part I: the dangers of flux correction. J Clim 8: 1325–1342

Neelin JD, Latif M, Allaart MAF, Cane MA, Cubasch U, Gates WL, Gent PR, Ghil M, Gordon C, Lau NC, Mechoso CR, Meehl GA, Oberhuber JM, Philander SGH, Schopf PS, Sperber KR, Sterl A, Tokiota T, Tribbia J, Zebiak SE (1992) Tropical air-sea interaction in general circulation models. Clim Dyn 7: 73–104

Pontaud M, Thual O (1998) Coupled processes for equatorial Pacific interannual variability. Q J R Meteorol Soc 124: 546: 527–555

Pontaud M, Céron JP, Pluviaud F and the CMIP1 participants (1998) Le sous-projet DIVCOP de CMIP: compilation des résultats, Note de l'ENM n°1, juin 1998, METEO-FRANCE Ecole Nationale de la Météorologie, 42 av, G Coriolis, 31057 Toulouse-cedex, France

Reynolds RW (1988) A real-time global sea surface temperature analysis. J Clim 1: 75–86

Stockdale T, Anderson D, Davey M, Delecluse P, Kattenberg, Kitamura Y, Latif M, Yamagata Y (1993) Intercomparison of tropical ocean GCMs. WCRP 79, WMO/TD-545

Terray L (1998) Sensitivity of climate to atmospheric physical parameterizations in a coupled ocean-atmosphere general circulation model. J Clim 11: 1633–1658

Vintzileos A, Sadourny R (1997) A general interface between an atmospheric general circulation model and underlying ocean and land surface models: delocalised physics scheme. Mon Weather Rev 125: 926–941

Vintzileos A, Delecluse P, Sadourny R (1999a) On the mechanisms in a tropical ocean-global atmosphere coupled general circulation model. Part I: mean state and seasonal cycle. Clim Dyn 15: 43–62

Vintzileos A, Delecluse P, Sadourny R (1999b) On the mechanisms in a tropical ocean-global atmosphere coupled general circulation model. Part II: interannual variability and its relation to the seasonal cycle. Clim Dyn 15: 63–80